Journal of Materials Chemistry A

Accepted Manuscript

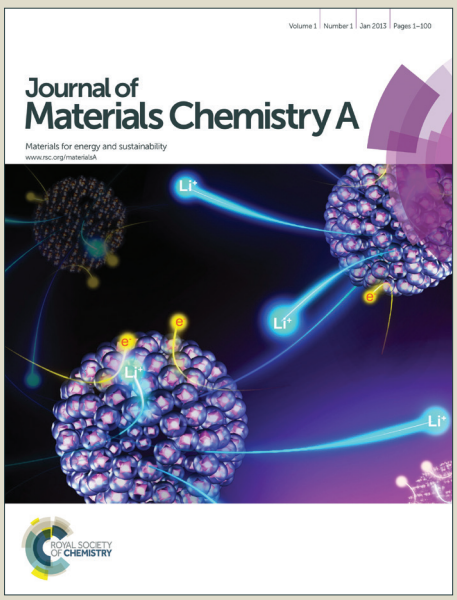

ROYAL SOCIETY OF CHEMISTRY

www.rsc.org/materialsA

Journal Name

RSCPublishing

ARTICLE

Multi-stimuli responsive smart elastomeric hyperbranched polyurethane/ reduced graphene oxide nanocomposites

Suman Thakur, Niranjan Karak*

Cite this: DOI: 10.1039/xoxxooooox

Received ooth January 2012,
Accepted ooth January 2012

DOI: 10.1039/xoxxooooox

www.rsc.org/

In this report, a tough elastomeric hyperbranched polyurethane/reduced graphene oxide (HPU/RGO) nanocomposite is fabricated by an in-situ polymerization technique. Reduction of graphene oxide was carried out by a green sonochemical approach using the combined effect of sonication and Fe^{3+} ions in presence of *Colocasia esculenta* leaves aqueous extract. It took only 3 min, while 8 min was required without sonication. Prepared RGO and nanocomposites were characterized by different spectroscopic and analytical tools. The nanocomposite demonstrated excellent thermal stability and mechanical properties such as tensile strength (27.8 MPa), tensile modulus (36.3 MPa) and toughness (116 MJm^{-3}). The nanocomposite also exhibited outstanding multi-stimuli responsive shape memory behaviour under direct sunlight, microwave (360 W) and heat energy (60 °C). The performance of the nanocomposite was dependent on the loading of RGO (0.5-2.5 wt%). Thus, these nanocomposites have tremendous potential to be used as advanced non-contact triggered smart materials for different applications including biomedical.

Introduction

Shape memory polymer (SMP) is a class of smart materials with capability of changing a predetermined shape to original in response to a suitable stimulus.[1] From the past decade, SMP has gained growing interest to material scientist due to its wide range of applications, ranging from biomedical to textiles.[2-5] In this context, polyurethane is one of the renowned SMPs due to its high recoverable strain (up to 400%), wide transition temperature range of shape recovery, high control of retraction and softening temperatures, inherent soft–hard segments and so forth.[6-9] At this juncture it is pertinent to mention that hyperbranched polymers have fascinated plentiful attention for their unique structural architectures and properties over their linear analogs.[10] Recently vegetable oil has demonstrated to be a unique feedstock to follow the dictates of green chemistry.[11] Among the genre of vegetable oils, castor oil (*Ricinus communis*) has carved a distinctive niche for its unique fatty acid composition and ready availability.[12] The monoglyceride of castor oil is found to be a better choice as a triol over the oil itself in the synthesis of hyperbranched polyurethane.[13]

Although, the shape-memory effects by direct heating are the most common and usual, but other stimuli such as light, magnetic and microwave (MW) have become gradually attractive. This is as a consequence of the capability to utilize reduced operating temperatures, be applied remotely, and result in localized shape-memory effects.[14-17] Commonly, light-induced shape-memory is attained either via light-induced heating or through photochemical reactions.[18] For example, Lendlein and his team used UV light as a stimulus to enable shape-memory effects by a photo-reversible cyclo-addition reaction.[19] Magnetic field induced SMPs are generally obtained by incorporating magnetic particles in the SMP matrix. The incorporation of the particle improved the mechanical properties as well as enabled to generate the shape memory effect under an alternating magnetic field.[20] In addition, MW is also an alternative choice as a noncontact stimulus for shape recovery of SMP. Recently Kalita and Karak reported that polyurethane/iron oxide nanocomposite exhibited excellent shape recovery under the MW power.[21] Even though remote shape-memory effects are developed using IR or UV irradiation, magnetic fields, MW as the stimuli; but most of the SMPs are poorly responded under such stimuli due to the low thermal conductivity of these materials. Therefore, good thermal conductive nanomaterials are required to improve uniform heat transfer ability to the SMP matrix and thereby facilitating efficient remote heating.[18] In this milieu, graphene, a two dimension carbon allotrope is the most attractive material for the above purpose as it has excellent thermal conductivity, electrical conductivity, MW absorbing capacity, light absorbing ability including sunlight and so forth.[22-24] Thus the unison of

vegetable oil based HPU and graphene as smart material may offer unique attribute to noncontact stimuli including sunlight, a natural ecofriendly and inexpensive practical stimulus.

After discovery of graphene by Geim and his co-worker, several methods are introduced to obtain graphene.[25-32] But, an efficient, eco-friendly and inexpensive methodology which allows the bulk production is still the prime requisites for the preparation of graphene. In this regard, chemical exfoliation of graphite by using strong oxidizing agents and followed by reduction of graphene oxide (GO) to reduced graphene oxide (RGO) is the most efficient approach for the preparation of graphene among others.[33] During the recent past, several greener reductants and protocols have been reported which effectively replacing the usage of hazardous chemical and methods for producing RGO.[34-42] Although phytoextracts (*Colocasia esculenta*, *Mesua ferrea* L. and *Citrus sinensis*) and tea solution can reduce GO at room temperature but took long time. In contrary, only a few literature have reported on green, fast and room temperature reduction of graphene oxide (GO). Akhavan et al. recently reported that antioxidant property of tea polyphenol augmented in presence of iron metal foil.[43] In this context, the reduction efficiency of aqueous *C. esculenta* extract may be enhanced in presence of various metal ions due to efficient complexation with polyphenols.

Therefore, in this report we investigated the reduction of GO by using *Colocasia esculenta* leaves aqueous extract in presence of various metal ions such as Fe^{3+} , Cr^{3+}, Cu^{2+} and Ni^{2+} under ambient conditions with and without sonication. Also hyperbranched polyurethane (HPU)/reduced graphene oxide (RGO) nanocomposites with different loading of RGO was fabricated and their mechanical properties as well as multi-stimuli responsive shape memory properties under thermal, MW and sunlight are delved into.

Experimental

Materials

Graphite flakes (60 meshes, purity 99%) and castor oil were obtained from Sigma-Aldrich, India. Concentrated sulphuric acid (98%), hydrogen peroxide (H_2O_2, 30%), glycerol, 1, 4-butanediol (BD), potassium permanganate ($KMnO_4$) and concentrated hydrochloric acid (30%) were purchased from Merck, India and used as received. Calcium oxide (CDH, India) and poly(ε-caprolactone) diol (PCL, Solvay Co., M_n= 3000 g mol^{-1}) were also used as received. *Colocasia esculenta* leaves were collected from the local area. Ferric chloride, nickel chloride, chromium chloride and copper chloride were used as metal ions source. Aqueous extract of *C. esculenta* and monoglyceride of the castor oil were prepared as the previously reported and GO was prepared based on modified Hummer's method.[13,33]

Sonochemical reduction of GO by aqueous extract of C. esculenta in presence different metal ions

GO brown suspension with concentration of 0.1 mg/mL was prepared by sonication for 30 min. To reduce this suspension of GO, an aqueous extract of *C. esculenta* with different metal ions separately was added to this GO suspension. Using a magnetic stirrer, the prepared GO–metal ion containing *C. esculenta* suspensions were stirred at 600 rpm at room temperature until the color of the solution turned to black from brown. The obtained black precipitate was repeatedly washed with MilliQ water to get RGO. Similar method was repeated to reduce the GO suspension under sonication (operating frequency 24 kHz) with standard sonotrode (tip-diameter 3 mm) in a high-intensity ultrasonic processor (UP200S, Hielscher Ultrasonics GmBH, Germany). A constant temperature of 293 K was maintained during the sonication.

Preparation of HPU/RGO nanocomposite

The polymerization reaction was carried out in a three-necked round bottomed flask, equipped with a nitrogen gas inlet, mechanical stirrer and Teflon septum. PCL (0.002 mol, 6 g), BD (0.004 mol, 0.36 g) and dispersion of RGO in DMAc (different wt%: 0.5, 1.5 and 2.5 with respect to total weight of nanocomposite) were taken in the flask with desired amount of xylene (maintaining solid content at 40%). After dissolving PCL, TDI (0.007 mol, 1.22 g) was added dropwise by help of a syringe into the reaction mixture at room temperature. Then the reaction was continued for 3 h at a temperature of (70±2) ºC to obtain the desired viscous mass, which was treated as the pre-polymer.

This pre-polymer was then cooled to room temperature and monoglyceride of castor oil (0.002 mol, 0.74 g) as a triol was added into it with the required amount of TDI (0.002 mol, 0.35 g). The temperature was then raised again to (110±2) ºC and continuously stirred for 2.5 h to complete the reaction as indicated by the absence of isocyanate band at 2270 cm^{-1} in the FTIR spectrum. This polymerization generates *in situ* biobased HPU/RGO nanocomposite.

HPU was also prepared without using RGO. HPU with 0.5, 1.5 and 2.5 wt% of RGO were encoded as HPU/RGO0.5, HPU/RGO1.5 and HPU/RGO2.5 respectively.

Material characterization

FTIR study was performed over the wavenumber range of 4000–400 cm^{-1} by a Nicolet (Madison, USA) FTIR impact 410 spectrophotometer using KBr pellets. XRD study was carried out at room temperature (*ca.* 25 °C) by a Rigaku X-ray diffractometer (Miniflex, UK) over the range of 2θ = 2–70° with scanning rate 2°/min. TGA was done by a thermal analyzer, TGA4000 (Perkin Elmer, USA) with a nitrogen flow rate of 30 mL/min at heating rate of 10 °C/min. Raman spectroscopy with SPEX 1403 double monochromator coupled to a SPEX 1442 was used. The samples were excited with an air cooled argon ion laser of wavelength 488 nm. Surface morphology of the prepared graphene was analyzed by transmission electron microscope (TEM, JEOL 2100X electron microscope) at operating voltage of 200 kV. The surface morphology of the fracture film of the nanocomposite was studied by a JEOL scanning electron microscope of model JSM-6390LV after gold coating on the

surface. Differential scanning calorimetry (DSC) was done by DSC 6000, Perkin Elmer, USA at 2 ^{o}C min^{-1} heating rate under the nitrogen flow rate of 30 mL min^{-1} from -20 to 120 ^{o}C. The tensile strength and elongation at break were measured with the help of the Universal Testing Machine (UTM), Jinan WDW 10, China with a 500 N load cell at crosshead speed of 20 mm/min. The impact strength measurement was carried out using falling weight method (standard ASTM D 1037) by an impact tester (S. C. Dey & Co., Kolkata, 100 cm is the maximum height). A weight of 850 g was allowed to fall on the mild steel plate coated film from minimum to maximum height up to which the film was not damaged.

In order to evaluate the shape memory behavior, the nanocomposite film was first heated at 60 °C for 5 min, and then stretched to twice of its original length (l_0), and the stretched length is denoted as l_1. Instantly, the stretched samples were placed in the ice-salt bath (-10 °C) for 5 min to release the stretch, and the length was measured as l_2. The shape recovery of the nanocomposite film was done by emerging the sample in warm water (60 °C) and the length obtained is denoted as l_3. The percentage of recovery was calculated by using the following equation.

Shape recovery (%) = $[(l_1-l_3)/l_0] \times 100$. ---------- (1)

To study the shape memory behavior under MW and direct sunlight, the bending test was performed. The sample was folded in ring form at 60 °C followed by quenching into an ice-salt bath for 5 min at -10 °C. Then the shape recovery of the nanocomposite films was achieved by exposing MW irradiation of 360 W for 30-60 s and direct sunlight (11 am-2 pm, at Tezpur University campus, altitude: 26.63 °N 92.8 °E in the month of March at sunny days, average temperature-34±1 °C and humidity-74±1 %) under ambient condition. The shape recovery was calculated using the following equation.

Shape recovery (%) = $\{(90-\theta)/90\} \times 100$ ---------- (2)

where θ in degree denotes the angle between the tangential line at the midpoint of the sample and the line connecting the midpoint and the end of the curved samples.

Result and discussions

Preparation of RGO

Reduction of GO was done using phytoextract in presence of different metal ions under ambient condition with and without sonication. However, the effective reduction was achieved only with Fe^{3+} ions, whereas the reduction efficiency was found to be insignificant for other metal ions (Cr^{3+}, Cu^{2+} and Ni^{2+}). The reduction in the presence of Fe^{3+} was ultrafast. It took only 3 min, though 8 min was required without sonication. This is a significant achievement as 8 h was required to reduce GO at room temperature when *C. esculenta* aqueous extract was used without metal ions.[33] After the reduction, the color of the GO solution turned from brown to black, indicative of the GO reduction and the prepared RGO precipitated from the solution as a result of the removal of hydrophilic functional groups. The attenuation of the reduction time simply suggested that the reduction ability of extract increased effectively in the presence of metal ion (Fe^{3+}) which resulted a quick reduction of GO.

Formation of the complex between Fe^{3+} and polyphenol was confirmed by taking the UV-visible spectra of Fe^{3+}, phytoextract and Fe^{3+}-phytoextract complex. Fe^{3+} and phytoextract showed UV absorbance at 289.5 and 267 nm respectively (Supporting Information, Fig. S1). But after mixing them a new absorbance peak was observed at 280 nm. This clearly reflects that complexation was taken placed. In the case of other studied metal ions, this type new absorption peak was not observed. The time for reduction was according to rate of complex formation. As Fe^{3+} can form a stable and stronger complex with polyphenol (PP) that was present in the extract compared to other metal ions and therefore it showed faster reduction.[43] During the complexation high amount of H^+ ions was released which changed the pH of the system. The pH of phytoextract and metal ion containing phytoextract were measured and found to be 6.03 and 3.21 respectively. In order to understand the effect of pH, a reduction was carried out by adjusting the pH of the mixed suspension at 3.2. But the same extent of reduction did not achieve even after 1h. This suggests that pH has no effective influence on the reduction process.

It was reported that ultrafast reduction was achieved by increasing the reduction potential difference between the two systems.[44] The reduction of GO with metals containing PP includes two half chemical reactions as shown below.

$$PP \longrightarrow OPP + 2H^+ + 2e^- \quad \text{------ (1)}$$

$$GO + aH^+ + be^- \longrightarrow RGO + cH_2O \quad \text{------- (2)}$$

where OPP is oxidized form of PP and a, b and c are numerical values. The corresponding electrode potential equations can be written as shown below.

$$E_{mC} = E^{o}_{mC} - \frac{RT}{2F} \ln \frac{1}{[OPP][H^+]^2} \quad \text{---------- (3)}$$

$$E_{GO} = E^{o}_{GO} - \frac{RT}{bF} \ln \frac{1}{[H^+]} = E^{o}_{GO} - 2.303 \frac{RT}{bF} pH \quad \text{---------- (4)}$$

where E^{o}_{mC} and E^{o}_{GO} are standard reduction potential of *C. esculenta* aqueous extract in the presence of Fe^{3+} and GO.

To confirm the role of reduction potential, the reduction potential values of GO (E_{GO}) at pH 6.0 and 3.2, *C. esculenta* aqueous extract (E_C) and *C. esculenta* aqueous extract in the presence of Fe^{3+} ions (E_{mC}) were measured. The values of $E_{GO(6)}$, $E_{GO(3.2)}$, E_C and E_{mC} were found to be -0.6V, -0.21V -1.6 V and -1.4 V respectively using Ag/AgCl as the reference electrode (Fig. 1). As E_{mC} mainly was dependent on the concentration of H^+ ion, the reduction potential, E_{mC} was found to be higher than E_C, though the concentration of free OPP decreased due to the complexation process. From equation 4, it is cleared that the reduction potential of GO is directly dependent on the pH of the system. Thus the E_{GO} value increased with the decreased of pH.

The difference between the reduction potential (ΔE°) of the systems: (i) PP without metal ion was 1.0V (1.6- 0.6V) and (ii) metal ion containing PP was 1.19V (1.4-0.21V), was slightly increased when complexation was taken placed. But this slight increase of ΔE° cannot influence the reduction process.

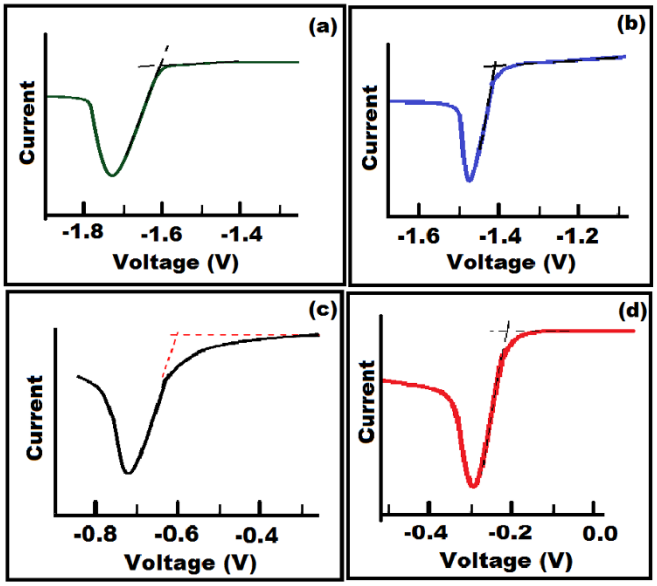

Fig. 1 Cyclic voltammograms of (a) *C. esculenta* aqueous extract, (b) *C. esculenta* aqueous extract in presence of Fe^{3+} ions, GO at pH (c) 6.0 and (d) 3.2.

These indicated that high rate of release of electron and formation of H^+ have more influence on the reduction. Plausible electron transfer mechanism for the reduction of GO is shown in the Scheme 1. Reduction was achieved by electron transfer as well as nucleophilic attack (SN^2) mechanism as shown in Scheme 1.

The reduction of GO was attained by sonochemical method which is a promising technique as ultrasound irradiation drives some special features such as elevated temperature, high pressure and rapid cooling rates etc. which are not occurred usually in the ordinary chemical reactions.[45] During the sonication small vacuum cavities are formed in the liquid medium. These cavities rapidly implode and generate microscopic shock waves. This cavitation is extremely powerful when the collective energy of all the imploding cavities is combined. Such cavities are formed and collapsed within microseconds and thereby releasing tremendous energy within the liquid medium. Thus, the use of ultrasound irradiation prevents the agglomeration of GO during the reduction which facilitates more reactions in between the layers of GO. This is really difficult to create in the conventional chemical reaction. In addition to this, the radicals produced in the reaction medium during ultrasonication also play a crucial role in the reduction of GO. Vinodgopal et al. demonstrated that the partial reduction of GO achieved after 4 h of ultrasound irradiation. The removal of oxygeneous groups of GO are facilitated by ultrasound irradiation due to enhance interactions of such groups with H^+ and e^- formed during complexation reaction.

In addition to that the effect of extreme temperature, pressure and high cooling rates due to the acoustic cavitation phenomena catalyzes the reduction within a shorter time. Also it is well known that GO is thermally unstable above 200 ºC, the high temperature produced during the ultrasound irradiation itself able to reduce the GO.

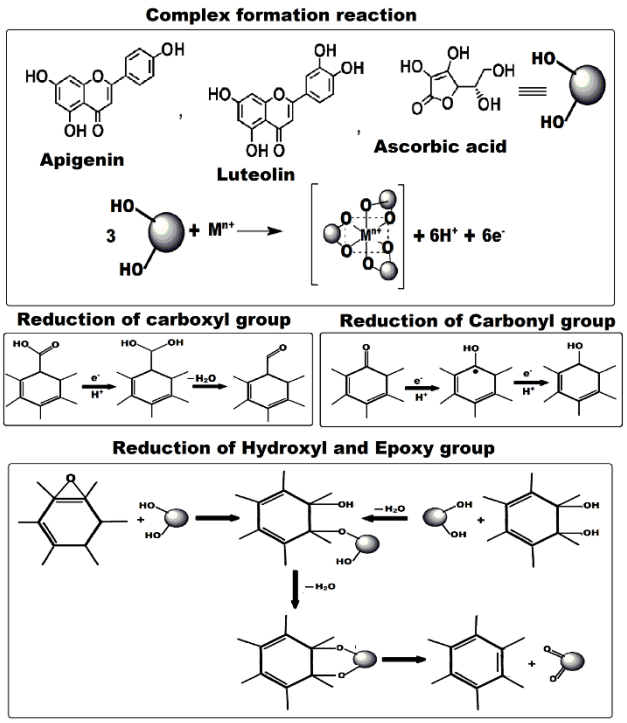

Scheme 1 Plausible electron transfer reduction mechanism of GO using *C. esculenta* leaves aqueous extracts in presence of Fe^{3+} ions.

Thus the ultrafast reduction of GO was achieved by the combined effect of ultrasonication and Fe^{3+} ions in the presence of *C. esculenta* leaves aqueous extracts. This may be due to fast complexation of phytochemicals with Fe^{3+} ions and generation of extreme reaction condition by ultrasonication. Hence, the reported approach for the reduction of GO was completed within 3 min.

Fig. 2a represents FTIR spectra of graphite, GO and RGO. As graphite has only carbonaceous structure, its FTIR spectrum contained a few bands for C=C moiety. In the spectrum of GO the presence of intense bands at 1719 cm^{-1} (for C=O stretching), 1221 cm^{-1} (for C–O–C stretching), 1050 cm^{-1} (for C–O stretching) and broad band at around 3400 cm^{-1} for hydroxyl group clearly indicated the presence of oxygen containing groups such as carbonyl, carboxylic, epoxy and hydroxyl in GO.[33] After the reduction of GO, disappearance of the afore-stated bands and relative decreased in the intensity of broad band at 3400 cm^{-1} for the hydroxyl group suggested the removal of most of such oxygen-containing groups.

XRD patterns of graphite, GO and RGO are shown in Fig. 2b. Pristine graphite exhibits a basal reflection (002) peak at $2\theta = 26.6°$ corresponding to d spacing of 0.335 nm. Upon oxidation of pristine graphite, in GO the (002) reflection peak shifts to the lower angle at $2\theta = 9.9°$, (d spacing = 0.892 nm).[35] Due to presence of the intercalation of water molecules and the formation of varieties of oxygen containing functional groups between the layers, the d spacing of graphite increased.

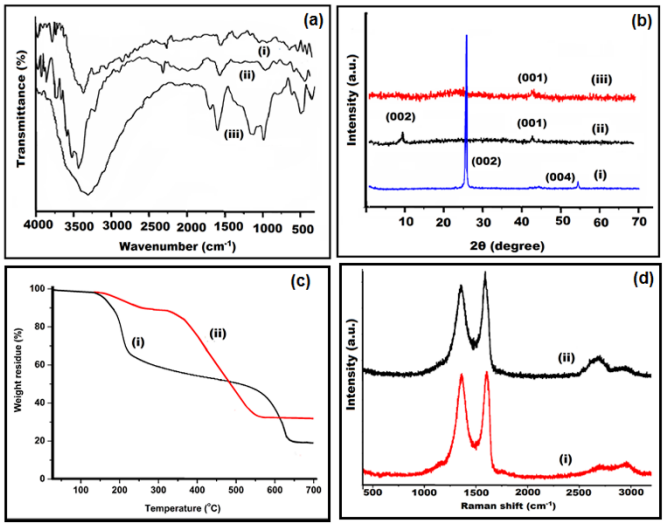

Fig. 2 (a) FTIR spectra of (i) graphite, (ii) RGO and (iii) GO, (b) XRD patterns of (i) graphite, (ii) GO and (iii) RGO, (c) TGA thermograms of (i) GO and (ii) RGO, and (d) Raman spectra of (i) GO and (ii) RGO.

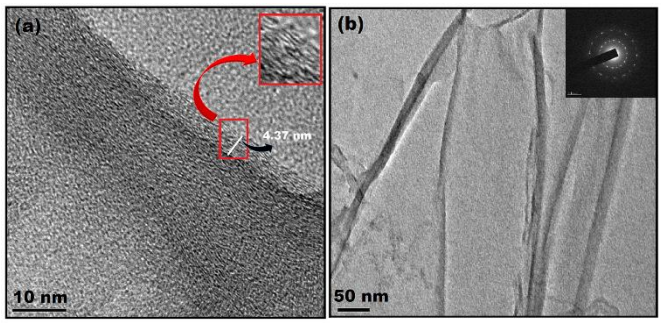

Fig. 3 HRTEM images of RGO (a) high-resolution (inset showing presence of planes) and (b) Low-resolution (inset showing SAED patterns of RGO).

In contrast to graphite and GO, RGO has a low intense broad peak centred at 2θ = 25° corresponding to d spacing of 0.36 nm which may be due to restacking of a few graphene layers. The close d spacing of RGO to pristine graphite and disappearance of peak at 2θ = 9.9° indicates that the oxygen containing groups of GO have been efficiently removed. In GO, a less intense peak at 43° was observed due to (100) plane of graphene.

Thermal stability of GO and RGO were examined by TGA (Fig. 2c). Both GO and RGO showed no significant weight loss near 100 °C, as the samples were completely dried before testing to eliminate the influence of absorbed moisture on the results. GO exhibited two steps degradation; the first step commencing at 170 °C due to the loss of remaining water molecules and such oxygenating functional groups. The second step degradation (540–630 °C) involves the pyrolysis of the remaining oxygen-containing groups as well as the burning of ring carbon.[34] RGO exhibits only a 7-8 wt% loss up to 250 °C, which was much lower than that of the GO, indicating a significantly decreased amount of oxygenated functional groups. RGO experiences 27% less weight loss in the 1st step of degradation than GO which is also an indication of degree of reduction.

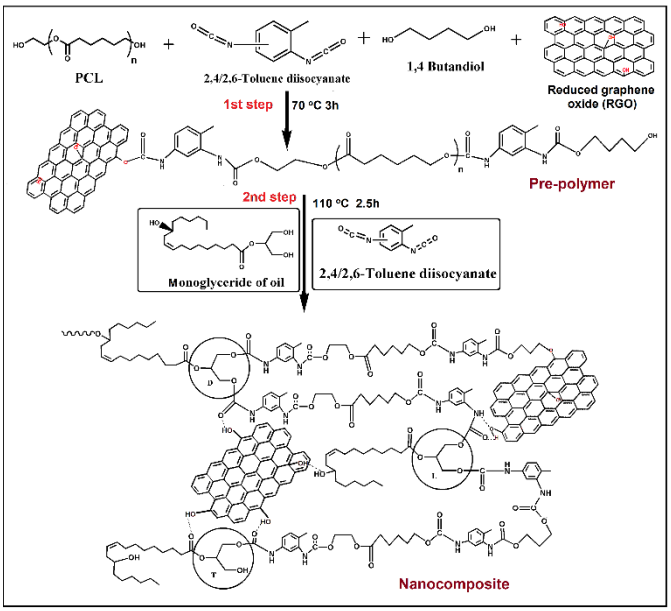

Scheme 2 Synthesis of HPU/RGO nanocomposite.

In Raman spectra of GO and RGO, two fundamental vibration bands were observed in range of 1100 to 1700 cm^{-1}. The G vibration mode, owing to the first-order scattering of E_{2g} phonons by sp^2 carbon of GO and RGO were found 1587 and 1584 cm^{-1} respectively while the D vibration band comes from a breathing mode of κ-point photons of A_{1g} symmetry of GO and RGO appeared at 1322 and 1327 cm^{-1} respectively (Fig. 2d).[37,38] After reduction of GO the intensity ratio of the D band to the G band (I_D/I_G) significantly increased. As D band arises due to sp^2 carbon cluster, so higher intensity of D band suggested presence of more isolated graphene domain in RGO in compare to GO and removal of oxygenating groups. Elemental composition of GO and RGO was evaluated by elemental analysis. Carbon to oxygen ratio (C/O) of RGO and GO were found to be 7.89 and 2.56 respectively which indicates the efficient reduction by phytochemicals in presence of Fe^{3+} ions.

Fig. 3a represents transmission electron microscope (TEM) images of RGO. RGO displays a crumpled morphology due to its high flexibility and large specific surface. The SAED pattern in the inset of Fig. 3b shows a typical semicrystalline ring composed of many diffraction spots, indicating the loss of long range ordering like graphitic structure in the RGO nanosheets.

HPU/RGO nanocomposite

Preparation of the nanocomposites

The HPU nanocomposites were synthesized by an A_2+B_3 technique using the monoglyceride of castor oil as a multifunctional moiety and RGO as reinforcing nanomaterial, as shown in Scheme 2. The crucial factors for the fruitful preparation of HPU nanocomposite are reaction time, concentration of the reactants, temperature and rate of addition of the triol moieties.[6]

RGO was incorporated in the 1st step of the polymerization process as a result it reacted with some of the isocyanate terminated prepolymer chains and provided strong interfacial interactions.[46] To avoid gel formation, the triol moiety was added slowly as a very dilute solution (15% in xylene). Also temperature of the reaction system was raised slowly from room temperature to 110 °C in the 2nd step of reaction.[10]

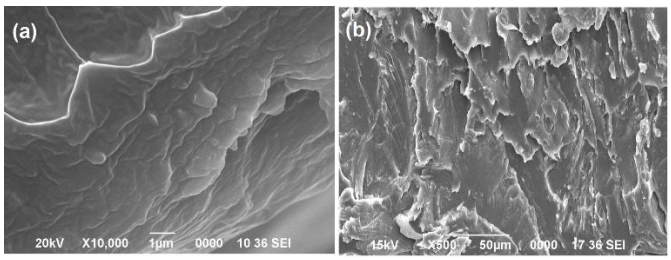

Fig. 4 SEM images of fracture surface (a) HPU/RGO 0.5 and (b) HPU/RGO 2.

Surface morphology of the nanocomposites

Fig.4 represents the SEM images of the fracture surface of the nanocomposites. Images clearly indicated micro-rough fracture surfaces of the nanocomposites. This is due to shear yielding or deformation of HPU matrix in between RGO.

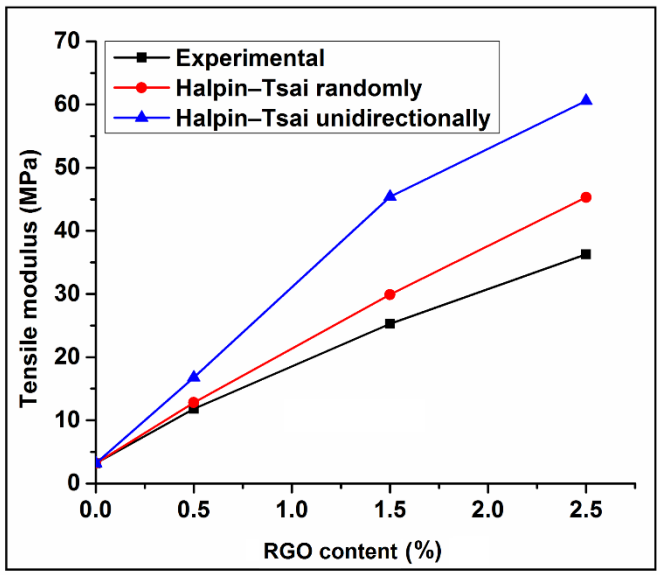

Fig. 5 comparison between the fitting results from the Halpin–Tsai model and the experimental data.

Mechanical properties

All the nanocomposite demonstrated excellent enhancement in mechanical properties like tensile strength, tensile modulus and toughness after incorporation of RGO in HPU matrix (Table 1). Dose dependent improvement in mechanical properties of the nanocomposites was observed. Formation of nanocomposite improves tensile strength, tensile modulus and toughness along with simultaneously improvement of elongation at break. The strong interfacial adhesion with good compatibility between HPU and RGO assists to achieve outstanding mechanical properties of the nanocomposite.[46] The possible strong chemical bonds formation between the remaining hydroxyl groups in RGO and isocyanate terminated prepolymer chains help to efficient transfer of the load from HPU to RGO in the nanocomposite. For this reason, the resulted nanocomposites exhibited such unusual improvement in the tensile strength. Owing to the presence of H-bonding, polar-polar interaction in the afore-stated covalent bond resulted stiffening effect on the hard domain of HPU, which subsequently enhances tensile modulus of the nanocomposite. The elongation at break was also increased due to alignment of polymer chains along the loading direction during initial stress and sliding of layers of RGO at high stress.[6] The scratch hardness was enhanced after incorporation of RGO into the HPU matrix. Thus toughness of the nanocomposite was also enhanced. HPU nanocomposites also absorbed the highest limit of impact energy due to the presence of soft segments in the HPU chain which dissipate the impact energy by segmental motions in their molecular chains in addition to their high strength.

The mechanical properties of polymeric nanocomposites mostly relies on the size, shape and orientation of the nanomaterials and load transfer efficiency from nanomaterial to polymer matrix. The Halpin-Tsai model is extensively used to investigate the distribution of 2-dimensional nanomaterial in the polymer matrix. Therefore, the model was used to evaluation the orientation of RGO sheets in the HPU nanocomposites. Details of the equations are given in the Supporting Information. Experimental and calculated Young's moduli of the nanocomposites at different RGO orientations are compared and shown in Fig. 5. The 3-dimensional random model better fitted the experimental results compared to the 2-dimensional aligned model. This result reflects that the RGO are randomly distributed in the HPU matrix. The deviation of Young's modulus progressively enlarged with increased the RGO content. As Young's moduli are obtained experimentally from the linear area of the stress–strain curves, alignment of RGO along the load direction is limited. Especially in HPU/RGO0.5, there is sufficient space for allowing RGO to arrange them in a random manner. Such space diminishes with the increase of RGO content and the interaction between adjacent RGO forces them to align along the force direction resulting in enlarged deviation to prediction of the random model.[6]

Table 1 Mechanical Properties of HPU and Nanocomposite Films

Sample	HPU	HPU/RGO0.5	HPU/RGO1.5	HPU/ RGO2.5
σ^a (MPa)	7.1±0.8	16.5±1.9	23.9±1.6	27.8±1.9
E^b(MPa)	3.2±0.4	11.8±1.4	25.3±1.1	36.3±3.2
ε (%)	690±35	894±36	951±46	988±34
T (MJ/m^3)	25.40±2.4	64.23±2.5	96.34±3.4	115.78±4.1
Scratch hardness (kg)	5±0.2	5.5±0.2	6±0.2	6.5±0.1
Impact strength (cm)	>100	>100	>100	>100

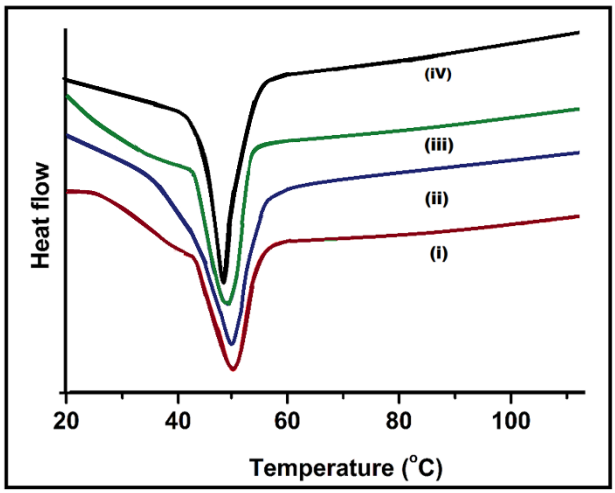

Fig. 6 DSC curves of (i) HPU/RGO2.5, (ii) HPU/RGO1.5, (iii) HPU/RGO0.5 and (iv) HPU.

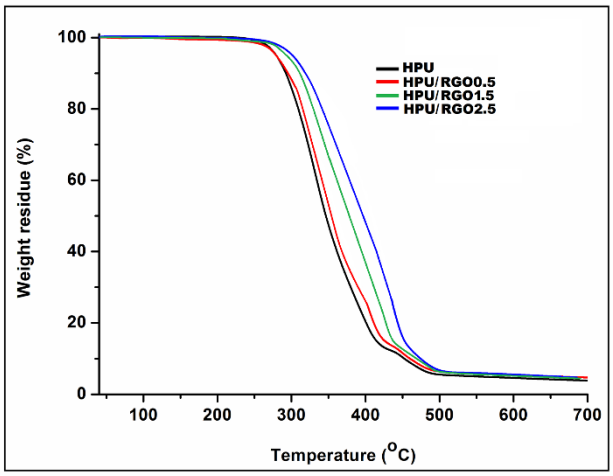

Fig. 7 TGA thermograms of HPU, HPU/RGO0.5, HPU/RGO1.5 and HPU/RGO2.5.

Thermal properties

DSC analysis was carried out to investigate the crystallization behavior of the nanocomposites.[6,46] The amount of crystalinity was found enhanced with loading of RGO (Table S1 in the Supporting Information). Also after incorporation of RGO, the melting temperature (T_m) of the soft segment of HPU was enhanced as shown in Fig. 6. Presence of RGO imposes restrictions on molecular mobility of HPU which resulted in the enhancement of T_m. This clearly indicated that RGO served as the nucleating agents and the presence of RGO improve the crystallization process by arranging of the polymer chains in a particular direction.

TGA was performed to validate the thermal stability of the nanocomposites (Fig. 7). All the nanocomposites showed two steps degradation patterns and the degradation temperatures of the nanocomposites enhanced with the amount of RGO loading. The improved thermo-stability of the nanocomposites is due to limited motion of the HPU chains by the different physico-chemical interactions such as covalent and noncovalent interactions with RGO.[6,46]

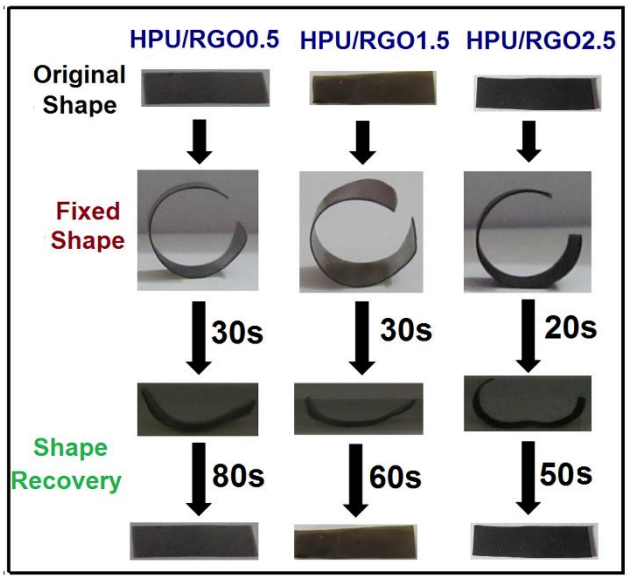

Fig 8. Shape memory behavior of the nanocomposites under MW stimulus.

Shape memory behavior

The multi-stimuli responsive shape memory behavior of the nanocomposites were evaluated under sunlight, microwave and thermal heating. Shape memory behaviours of the nanocomposite by MW and sunlight are shown in Fig. 8. Entire nanocomposite exhibited excellent shape fixity and recovery under the mentioned stimulus. Shape recovery values of the nanocomposite films were faster and more efficient upon exposure to MW and sunlight compared to the thermal stimulus. This may be due to excellent MW and sunlight absorbing capacity of RGO. Shape recovery time and ratio under different stimuli are tabulated in Table 2.

Table 2. Shape memory properties of the nanocomposites

Stimulus		HPU/RGO 0.5	HPU/RGO 1.5	HPU-IO/RGO 2.5
MW	Shape recovery time (s)	80	60	50
	Shape recovery ratio (%)	95.2	96.6	98.3
Sunlight	Shape recovery time (min)	2.5	1.5	1.0
	Shape recovery ratio (%)	96.4	97.6	98.9
Thermal	Shape recovery time (min)	5	4.5	3
	Shape recovery ratio (%)	95.2	96.8	97.6

The shape recovery time was found decreased with the increase of RGO content in the nanocomposites. RGO created a large amount of stored elastic strain energy owing to presence of strong interfacial interactions with the HPU matrix.[6] This helped the nanocomposites to attain a high recovery speed due to the release of stored elastic strain. Energy absorbing capacity from

different stimuli also enhanced with increase of the amount of RGO which is another important factor for the fast recovery.

Conclusions

In summary, a green ultrafast reduced GO and its nanocomposites with HPU were fabricated by an in-situ polymerization technique. The resultant nanocomposite exhibited excellent thermo-mechanical properties and multi-stimuli responsive shape memory behavior. The study also confirmed the selectivity of metal ions on the reduction to RGO.

Acknowledgements

The authors express their gratitude to SAP (UGC), India through grant No. F.3-30/2009(SAP-II) and FIST program-2009 (DST), India through the grant No.SR/FST/CSI-203/209/1 dated 06.05.2010. RSIC, NEHU, Shillong is gratefully acknowledged for the TEM imaging.

Notes and references

Advanced Polymer and Nanomaterial Laboratory, Department of Chemical Sciences, Tezpur University, Tezpur 784028, India.
Fax: +91 3712-267006; Tel:+91 3712-267327;
E-mail: karakniranjan@yahoo.com (N. Karak)

†Electronic Supplementary Information (ESI) available: Thermal properties of the nanocomposite and, UV-visible spectra of phytoextract and Fe3+ solution are given in the supporting information.

1. A. Lendlein and R. Langer, *Science* 2002, **296,** 1673– 1676.
2. A. Lendlein and V. P. Shastri, *Adv. Mater*. 2010, **22**, 3344–3347.
3. D. Ratna and J. K. Kocsis, *J. Mater. Sci.* 2008, **43**, 254– 269.
4. P. Mather, X. Luo and I. Rousseau, *Annu. Rev. Mater. Res.* 2009, **39**, 445– 471.
5. C. M. Yakacki, R. Shandas, D. Safranski, A. M. Ortega, K. Sassaman, and K. Gall, *Adv. Funct. Mater*. 2008, **18**, 2428–2435.
6. S. Thakur and N. Karak, *RSC Adv.* 2013, **3**, 9476-9482.
7. J. Zhu**,** S. Wei**,** N. Haldolaarachchige, D. P. Young, and Z. Guo, *J. Phys. Chem. C*, 2011, **115** (31), 15304–15310.
8. Ding, H. Wei, J. Zhu, Q.He, X. Yan, S. Wei, Z. Guo, *Energy Environ. Focus*, 2014, **3**(1), 85- 93.
9. H. Wei, D. Ding, S. Wei and Z. Guo, *J. Mater. Chem. A*, 2013, **1**, 10805-10813.
10. S. Barua, G. Dutta and N. Karak, *Chem. Eng. Sci.* 2013, **95**, 138–147.
11. H. Kalita and N. Karak, *J. Appl. Polym. Sci.* 2014, 131, DOI: 10.1002/app.39579.
12. S. Allauddin, R. Narayan and K. V. S. N. Raju, *ACS Sustainable Chem. Eng.* 2013, **1** (8) 910-918.
13. S. Thakur and N. Karak, *Prog. Org. Coat.* 2013, **76**, 157– 164.
14. S. K. Ahn, P. Deshmukh and R. M. Kasi, *Macromolecules* 2010, **43**, 7330–7340.
15. Y. Yu and T. Ikeda, *Macromol. Chem. Phys.* 2005, **206**, 1705– 1708.
16. C. M. Yakacki, N. S. Satarkar, K. Gall, R. Likos and J. Z. Hilt, *J. Appl. Polym. Sci.* 2009, **112**, 3166– 3176.
17. H. Kalita and N. Karak, *Polym. Adv. Technol*. 2013, DOI: 10.1002/pat.3149.
18. J. R. Kumpfer and S. J. Rowan, *J. Am. Chem. Soc*., 2011, **133** (32), 12866–12874.
19. A. Lendlein, H. Jiang, O. Jeunger, and R. Langer, *Nature* 2005, **434**, 879–882.
20. T. Weigel, R. Mohr and A. Lendlein, *Smart Mater. Struct.* 2009, **18**, 1–9.
21. H. Kalita and N. Karak, *Polym. Int.* 2014, DOI: 10.1002/pi.4674.
22. O. Akhavan, E. Ghaderi and A. Esfandiar, *J. Phys. Chem. B* 2011, **115**, 6279–6288.
23. X. Zhao, Z. Zhang, L. Wang, K. Xi, Q. Cao, D. Wang, Y. Yang, and Y. Du, *Sci. Rep.* 2013, **3**, DOI: 10.1038/srep03421.
24. M. Bernardi, M. Palummo, and J. C. Grossman, *Nano Lett.* 2013, **13**, 3664-3670.
25. L. Shao, S. Quan, Y. Liu, Z. Guo, Z. Wang, *Mater. Lett.* 2013, **107**(15), 307-310.
26. J. Zhu, M. Chen, Q. He, L. Shao, S. Wei and Z. Guo, *RSC Adv.* 2013, **3** (45), 22790 - 22824.
27. H. Gu, X. Zhang, H. Wei, Y. Huang, S. Wei and Z. Guo, *Chem. Soc. Rev.* 2013, **42**, 5907-5943.
28. L. Shao, X. Chang, Y. Zhang, Y. Huang, Y. Yao and Z. Guo, *Appl. Surf. Sci.* 2013, **280**(1), 989–992.
29. X. Zhang, O. Alloul, Q. He, J. Zhu, M. J. Verde, Y. Li, S. Wei and Z. Guo, *Polymer* 2013, **54**(14), 3594–3604.
30. J. Zhua, M. Chena, H. Quab, Z. Luoc, S. Wud, H. A. Coloradoe, S. Wei and Z. Guo, *Energy Environ. Sci.* 2013, **6**, 194-204.
31. J. Zhu, R. Sadu, S. Wei, D. H. Chen, N. Haldolaarachchige, Z. Luo, J. A. Gomes, D. P. Young and Zhanhu Guo, *ECS J. Solid State Sci. Tech.* 2012, **1**(1), M1-M5.
32. S. Park and R. S. Ruoff, *Nat. Nanotechnol*. 2009, **4**, 217–224.
33. S. Thakur and N. Karak, *Carbon* 2012, **50**, 5331– 5339.
34. Y. Wang, Z. Shi and J. Yin, *ACS Appl. Mater. Interface* 2011, **3**, 1127–1133.
35. T. Kuila, S. Bose, P. Khanra, A. K. Mishra, N. H. Kim and J. H. Lee, *Carbon* 2010, **50**,914–921.
36. L. J. Cote, R. Cruz-Silva and J. Huang, *J. Am. Chem. Soc.* 2009, **131**, 11027–11032.
37. Y. Zhou, Q. Bao, L. Tang, Y. Zhong and K. P. Loh, *Chem. Mater.* 2009, **21**, 2950–2956.
38. G. Williams, B. Seger and P. V. Kamat. *ACS Nano* 2008, **2**, 1487–1491.
39. A. Esfandiar, O. Akhavan and A. Irajiza, *J. Mater. Chem.* 2011, **21**, 10907.
40. S. Bose, T. Kuila, A. K. Mishra, N. H. Kim and J. H. Lee, *J. Mater. Chem.* 2012, **22**, 9696–9703.
41. S. Thakur, G. Das, P. K. Raul and N. Karak, *J. Phys. Chem. C* 2013, **117** (15), 7636–7642.
42. O. Akhavan, M. Kalaee, Z.S. Alavi, S.M.A. Ghiasi and A. Esfandiar, *Carbon* 2012, **50**, 3015– 3025
43. N. R. Perron, H. C. Wang, S. N. DeGuire, M. Jenkins, M. Lawson and J. L. Brumaghim, *Dalton Trans.* 2010, **39,** 9982–9987.
44. X. Mei, H. Zheng and J. Ouyang, *J. Mater. Chem.* 2012, **22**, 9109-9116.
45. K. Krishnamoorthy, G. Kim and S.J. Kim, *Ultrason. Sonochem.* 2013, **20**, 644–649.
46. S. Thakur and N. Karak, *ACS Sustainable Chem. Eng.* 2014, **2**, 1195−1202.

.

A table of contents entry

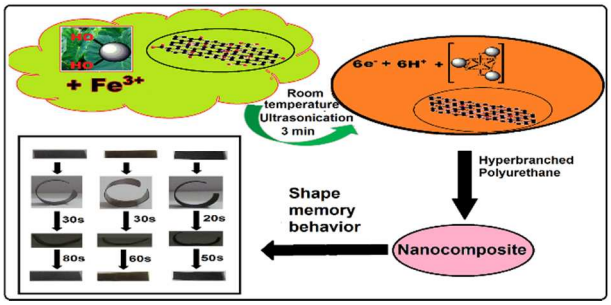

Multi-stimuli responsive smart elastomeric hyperbranched polyurethane/reduced graphene oxide nanocomposite is fabricated using ultrafast reduced graphene oxide